JACC: CARDIOVASCULAR IMAGING VOL. 2, NO. 5, 2009

ISSN 1936-878X/09/$36.00
PUBLISHED BY ELSEVIER INC. DOI:10.1016/j.jcmg.2008.08.009

Macrophage-Specific Lipid-Based Nanoparticles Improve Cardiac Magnetic Resonance Detection and Characterization of Human Atherosclerosis

Michael J. Lipinski, MD,*†‡§‖ Juan C. Frias, PHD,*†¶ Vardan Amirbekian, MD,*†#
Karen C. Briley-Saebo, PHD,*† Venkatesh Mani, PHD,*† Daniel Samber, PE,*†
Antonio Abbate, MD,§ Juan Gilberto S. Aguinaldo, MD,*† Davis Massey, DDS, MD, PHD,**
Valentin Fuster, MD, PHD,‡ George W. Vetrovec, MD,§ Zahi A. Fayad, PHD*†‡

New York, New York; Richmond and Charlottesville, Virginia; Valencia, Spain; and Boston, Massachusetts

OBJECTIVES We sought to determine whether gadolinium (Gd)-containing lipid-based nanoparticles (NPs) targeting the macrophage scavenger receptor-B (CD36) improve cardiac magnetic resonance (CMR) detection and characterization of human atherosclerosis.

BACKGROUND Gd-containing lipid-based NPs targeting macrophages have improved MR detection of murine atherosclerosis.

METHODS Gadolinium-containing untargeted NPs, anti-CD36 NPs, and nonspecific Fc-NPs were created. Macrophages were incubated with fluorescent targeted and nontargeted NPs to determine uptake via confocal microscopy and inductively coupled plasma mass spectroscopy (ICP-MS) quantified Gd uptake. Human aortic specimens were harvested at autopsy. With a 1.5-T scanner, T1, T2, and PDW 3-dimensional scans were performed along with post-contrast scans after 24 h incubation. The T1 and cluster analyses were performed and compared with immunohistopathology.

RESULTS The NPs had a mean diameter of 125 nm and 14,900 Gd-ions, and relaxivity was 37 $mmol/l^{-1}s^{-1}$ at 1.5-T and 37°C. Confocal microscopy and ICP-MS demonstrated significant in vitro macrophage uptake of targeted NPs, whereas non-targeted NPs had minimal uptake. On T1 imaging, targeted NPs increased contrast-to-noise ratio (CNR) by 52.5%, which was significantly greater than Fc-NPs (CNR increased 17.2%) and nontargeted NPs (CNR increased 18.7%) ($p = 0.001$). Confocal fluorescent microscopy showed that NPs target resident macrophages, whereas the untargeted NPs and Fc-NPs are found diffusely throughout the plaque. Targeted NPs had a greater signal intensity increase in the fibrous cap compared with non-targeted NPs.

CONCLUSIONS Macrophage-specific (CD36) NPs bind human macrophages and improve CMR detection and characterization of human aortic atherosclerosis. Thus, macrophage-specific NPs could help identify high-risk human plaque before the development of an atherothrombotic event. (J Am Coll Cardiol Img 2009;2:637–47) © 2009 by the American College of Cardiology Foundation

From the *Translational and Molecular Imaging Institute, †Imaging Science Laboratories, Department of Radiology, ‡The Zena and Michael A. Wiener Cardiovascular Institute, The Marie-Josée and Henry R. Kravis Cardiovascular Health Center, Department of Internal Medicine, Division of Cardiology, Mount Sinai Medical Center, New York, New York; §VCU Pauley Heart Center, Virginia Commonwealth University, Richmond, Virginia; ‖Department of Internal Medicine, University of Virginia Health System, Charlottesville, Virginia; ¶Instituto de Ciencia Molecular, University of Valencia, Valencia, Spain; #Department of Radiology, Brigham and Womens Hospital, Boston, Massachusetts; and the **Department of Pathology, Virginia Commonwealth University Health

JACC: CARDIOVASCULAR IMAGING, VOL. 2, NO. 5, 2009
MAY 2009:637–47

The clinical manifestations of atherosclerosis, namely myocardial infarction and stroke, remain the leading cause of morbidity and mortality in the U.S. (1) and in Western society. Because the majority of acute coronary syndromes occur from rupture of lesions <50% stenosed (2,3), identification of high-risk lesions in individuals before rupture can be challenging. Detection of these lesions by conventional means of assessing atherosclerosis, such as coronary angiography, remains limited (4). Atherosclerotic lesions prone to rupture were shown to have a thin fibrous cap, a large lipid core, and a large number of inflammatory cells including macrophage-derived foam cells (5,6). Therefore, development of noninvasive imaging agents that target components of atherosclerotic plaque might enable improved detection and characterization of plaque (7).

ABBREVIATIONS AND ACRONYMS

Apo = apolipoprotein
CD204 = a class A macrophage scavenger receptor
CD36 = a class B macrophage scavenger receptor
CMR = cardiac magnetic resonance
CNR = contrast-to-noise ratio
DAPI = 4′,6′-diamidino-2-phenylindole hydrochloride
DPPE-NBD = 1,2-Dipalmitoyl-sn-glycero-3-phosphoethanolamine-N-7-nitro-2-1,3-benzoxadiazol-4-yl
Gd = gadolinium
ICP-MS = inductively coupled plasma mass spectroscopy
MSR = macrophage scavenger receptor
NP = nanoparticle
PBS = phosphate-buffered solution
PDW = proton-density-weighted
RPE = phycoerythrin
SNR = signal-to-noise ratio
SPIO = superparamagnetic iron oxide particle

In an effort to create cardiac magnetic resonance (CMR) contrast agents that deliver a large payload of paramagnetic particles, we developed gadolinium (Gd)-loaded lipid-based nanoparticles (NPs) that can be modified to target biological ligands. As previously described, Gd-loaded NPs modified with antibodies targeting macrophage scavenger receptor (MSR)-A (or CD204) not only improved in vitro CMR detection of macrophages but also improved ex vivo detection of murine atherosclerosis and macrophage density (8). Recently, NPs targeting the MSR-A were shown to improve in vivo detection of murine atherosclerosis with a high correlation between the signal intensity on CMR and the number of macrophages in the region of interest (9). CD36, a class B scavenger receptor, has been shown to have an important role in oxidized lipoprotein uptake, which might explain its increased expression in atherosclerosis. Therefore, we set out to determine whether Gd-labeled NPs targeting CD36 bind to macrophages and improve MR detection and characterization of human atherosclerosis.

METHODS

NPs formulation. The NPs were made from phospholipids [palmitoyl-oleoyl phosphatidylcholine (POPC), 1,2-dipalmitoyl-sn-glycero-3-phosphoethanolamine-N-7-nitro-2-1,3-benzoxadiazol-4-yl (DPPE-NBD), 1,2-dipalmitoyl-sn-glycero-3-phosphoethanolamine-N-biotinyl (DPPE-Biotin)], a surfactant (Tween 80), and an aliphatic gadolinium complex (Gd-DOTA-BSA, Gateway Chemical, St. Louis, Missouri) as previously described (8,10). The POPC and the Gd complex were dissolved in a 1:1 chloroform/methanol solution (5 ml). Evaporation under nitrogen flux yielded a thin film that was then rehydrated in hot water (2 ml, 70°C). This solution was sonicated for 15 min at 70 W at 90% cycle duty while the temperature was kept at 65°C with a thermostatic bath. After sonication, Tween 80 was added, followed by another 15 min of sonication. Green fluorescent NBD-labeled untargeted NPs were obtained by adding 2 mol % of fluorescent phospholipid DPPE-NBD to the formulation, and red fluorescent rhodamine-labeled untargeted NPs were obtained by adding 2 mol % of fluorescent phospholipid DPPE-rhodamine to the formulation. Biotinylated NPs were prepared by addition of 0.5 mol % of DPPE-Biotin to the reaction mixture. Biotinylated rabbit anti-human polyclonal antibodies to human CD36 (IgG, Novus Biologicals, Littleton, Colorado) and biotinylated ChromPure rabbit IgG fragment crystallizable (Fc) region (Jackson Immunoresearch, West Grove, Pennsylvania) were used to make targeted NPs s and Fc-NPs, respectively. Targeted NPs and Fc-NPs were prepared by adding approximately 1.9×10^{-10} mol/l of biotinylated NPs dissolved in phosphate buffered solution (PBS) to 9.7×10^{-10} mol/l of streptavidin (Sigma-Aldrich, St. Louis, Missouri), and the vial was shaken for 30 min. Then 2.3×10^{-9} mol/l of biotinylated anti-CD36 or Fc fragment dissolved in PBS were added to the vial and shaken for another 3.5 h. This enabled the antibody to bind to the NP via a biotin-streptavidin-biotin bridge. Therefore the solution containing targeted NPs and Fc-NPs had a ratio of 10 parts anti-CD36 or Fc-portion to 5 parts streptavidin to 1 part NP, ensuring that excess antibody is available for each particle.

System, Richmond, Virginia. This study was supported in part by NIH/NHLBI ROI HL71021, NIH/NHLBI HL078667 (to Dr. Fayad), and the Stanley J. Sarnoff Endowment for Cardiovascular Research, Inc. (to Dr. Amirbekian). The MSSM-Microscopy Shared Resource Facility is supported by funding from NIH-NCI shared resources Grant R24 CA095823, and NSF Major Research Instrumentation Grant DBI-9724504.

Manuscript received July 17, 2008, accepted August 19, 2008.

The NPs were characterized by photon correlation spectroscopy performed with a Malvern multiangle dynamic laser light scattering system at room temperature, and inductively coupled plasma-mass spectrometry (ICP-MS) measurements provided the number of Gd ions/particle (11). The relaxivity of contrast agents was determined at 37°C with a 1.5-T clinical scanner. Two formulations of NPs were created for this study.

In vitro protocol. Human peripheral blood THP-1 monocytes were isolated with well-established adhesion methods (12). The monocytes were activated by incubation with human recombinant macrophage colony-stimulating factor (1 μg/ml; Sigma). The activated monocytes/macrophages were plated for 1 week in Dulbecco's modified Eagle medium containing fetal calf serum. The cells were washed and further activated by the addition of oxidized low-density lipoprotein (5 μg/ml, malondialdehyde-modified low-density lipoprotein), as previously described (13). Twenty-four hours after the addition of malondialdehyde-modified low-density lipoprotein, the cells were washed with fresh culture medium, and the NPs were added at a concentration of 1 mmol/l Gd. To evaluate the competition between the targeted and untargeted particles, cells were incubated as follows: 1) cells incubated with 1 mmol/l Gd of NBD-labeled untargeted particles; 2) cells incubated with 1 mmol/l Gd rhodamine-labeled targeted particles (CD36); 3) cells incubated with 1 mmol/l Gd NBD-labeled untargeted particles and 1 mmol/l Gd rhodamine-labeled targeted particles (CD36); and 4) control cells. All cells were then incubated for 24 h at 37°C. After incubation, the cells were washed (3×) with PBS and scraped in 0.25 ml of PBS. We then transferred 5 μl of the cell suspension to a slide and smeared with blood smearing techniques. The cells were fixed to the slide (4% paraformaldehyde) and washed with PBS. We added 5 μl of 4',6'-diamidino-2-phenylindole hydrochloride (DAPI), the slides were mounted, and confocal microscopy was performed after 24 h. The remaining 0.245 ml of cells were measured for cell number (bright light counting chamber) and sent for ICP-MS for Gd quantification. The resultant Gd concentrations (μg/ml) were then normalized to the cell numbers present.

Ex vivo protocol. Aortas with moderate to severe atherosclerotic disease were harvested from subjects at the time of autopsy. Each piece of aorta was divided into 3 equal sections with transverse cuts across the arterial lumen, preserving the lumen and vascular wall. Each section had an approximate height of 1 cm. For this experiment, 16 sections of aorta were selected from a total of 6 different subjects (4 different aortas yielding 3 sections each, and 2 different aortas yielding 2 sections each). The experimental design was for 6 aorta sections to be incubated with CD36-labeled NPs, 6 aorta sections to be incubated with untargeted particles, and 4 aorta sections to be incubated with unspecific Fc-particles. Before imaging, the sections of aorta were removed from formalin, cleaned, dabbed dry, and placed in Fomblin solution (perfluoropolyether; Ausimont USA Inc., Thorofare, New Jersey) for CMR. Fomblin does not have a residual MR signal and does not interfere with the biological tissue signal (14). After the initial pre-contrast CMR, the aorta sections were removed, dabbed dry, placed in individual plastic containers with PBS, and the solution of targeted NPs, untargeted NPs, or Fc-NPs was added. The plastic containers were covered and placed on a shaker for incubation at 4°C for 24 h. After incubation, the aorta sections were removed from the solution, cleaned, dabbed dry, placed in fomblin in their original positions from the pre-contrast imaging, and were imaged.

Ex vivo imaging. Pre-contrast and post-contrast imaging of the aorta sections was performed with a Siemens Sonata 1.5-T MR system. Sixteen contiguous axial images were obtained with T1, T2, and proton-density weighted (PDW) spin echo sequences. This enabled 3-dimensional multicontrast analysis of the aortas. The T1 images were obtained with a repetition time of 300 ms and an echo time of 9 ms, T2 images were obtained with a repetition time of 2,000 ms and an echo time of 55 ms, and PDW images were obtained with a repetition time of 2,000 ms and an echo time of 9 ms. The images had a slice thickness of 0.5 mm, matrix size of 512 × 512 pixels, field of view of 12.8 × 12.8 cm, and a resolution of 0.25 × 0.25 mm. The T1 sequence acquisition time was 9 min, T2 acquisition time was 15 min, and PDW sequence acquisition time was <15 min. The receiver gain was automatically calculated by the CMR system.

Confocal fluorescent microscopy. Confocal laser scanning microscopy was performed at the MSSM-Microscopy Shared Resource Facility with the appropriate light sources and filter sets on the control aortas and aortas incubated with fluorescent CD36-labeled, untargeted, and unspecific particles. All arteries were washed and frozen in optical cutting temperature compound Tissue Tek, Sakura Finetech, Tokyo, Japan). Ten-micron sections were cut and mounted on slides and stained with phycoerythrin (RPE)-labeled anti-CD68 (excitation

wavelength: 532 to 561 nm, emission wavelength: 578 to 610 nm) and DAPI (excitation wavelength: 385 to 400 nm, emission wavelength: >450 nm). Anti-CD68 is an antibody directed against lysosomal glycoproteins of macrophages (15), whereas DAPI is known to bind DNA in cellular nuclei (16). The NBD-labeled untargeted NPs had an excitation wavelength of 460 nm and emission wavelength of 534 nm. Light microscopy was performed with and without hematoxylin and eosin staining to allow histopathological comparison with corresponding MR images.

Image analysis. Three-dimensional T1 image analysis was performed for each aorta. Sixteen contiguous slices were obtained, and analysis was performed on contiguous slices in which there was no disruption of the aortic wall (the aorta was present as a complete circle). Eight regions of interest spanning the intima, media, and adventitia of equal size in each aorta for pre-contrast slices were selected, and the corresponding regions of interest were selected for the corresponding post-contrast slice. The mean signal intensity for the 8 regions of interest was calculated for each slice along with the signal intensity of the noise and the SD of the noise. The signal-to-noise ratio (SNR) was calculated by the following equation:

$$\text{SNR} = \text{mean signal intensity of 8 regions of interest} / \text{SD of the noise} \quad [1]$$

The mean pre- and post-contrast SNR of each aorta was then determined by taking the average of the SNR for each slice for pre- and post-contrast images, respectively. The change in pre- and post-contrast SNR, also known as contrast-to-noise ratio (CNR), was determined by the following equation:

$$\text{CNR} = ([\text{Post-Con SNR} - \text{Pre-Con SNR}]/\text{Pre-Con SNR}) \times 100 \quad [2]$$

Composition images were created by merging red, green, and blue images in which the T1 image was converted to a red image, T2 was converted to a green image, and PDW was converted to a blue image (14). The histopathological section for each aorta was then compared with the matching composition image. Type IV and V lesions as defined by Stary et al. (17) were identified on histopathological images. A dense accumulation of extracellular lipid that occupies an extensive but well-defined region of the intima was used to define a lipid core (17). The tissue layer between the lipid core and the endothelial surface was defined as the fibrous cap (17). Cluster analysis was performed by determining the T1 pre-contrast and post-contrast SNR for each aorta in regions of lipid core and fibrous cap.

Statistical analysis. Comparison of SNR between pre- and post-contrast T1 images was performed with paired Student *t* test analysis. One-way analysis of variance (ANOVA) was performed to compare between treatment groups for pre-contrast SNR and post-contrast SNR, respectively. A 2-way ANOVA was performed to compare the CNR of particular imaging agents to determine superiority of 1 agent compared with another. Pair-wise comparisons were made without adjustment for Type I

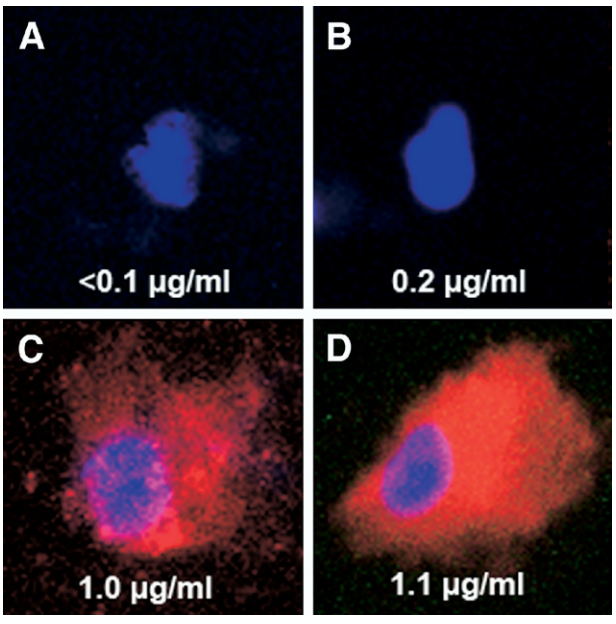

Figure 1. Confocal Microscopy Demonstrating In Vitro Macrophage Uptake of NPs

Confocal microscopy merged images (nitro-2,1,3-benzoxadiazol-4-yl [NBD] = **green**, rhodamine = **red**, 4′,6′-diamidino-2-phenylindole hydrochloride [DAPI] = **blue**) at 100× of activated human monocytes incubated in vitro with control **(A)**, NBD-labeled untargeted nanoparticles (NPs) **(B)**, rhodamine-labeled NPs targeting macrophage scavenger receptor-B (CD36) **(C)**, and with both NBD-labeled untargeted NPs and rhodamine-labeled NPs targeting CD36 **(D)** and stained with DAPI. Included with each image in the bottom of the panel is the Gd concentration (µg/ml) normalized to the cell numbers present. As seen in **A**, the nuclei of the control cells appear **blue**, and there was no significant gadolinium (Gd) present as expected. In cells incubated with untargeted NBD-labeled NPs **(B)**, there was trivial green fluorescence seen and minimal uptake of Gd as seen on inductively coupled plasma mass spectroscopy (ICP-MS). Cells incubated with rhodamine-labeled NPs targeting C36 **(C)** demonstrated significant red fluorescence corresponding with cellular uptake of targeted NPs, and ICP-MS also demonstrated significant Gd uptake. As seen in **D**, there was again significant uptake of rhodamine-labeled NPs targeting CD36 but trivial uptake of untargeted NBD-labeled NPs. The cellular uptake of Gd as shown on ICP-MS in **D** appears similar to the sum of Gd concentrations for **B and C**.

error rates. Results are shown as mean ± SD. Values of $p < 0.05$ were considered significant. Number Crunching System Software (Salt Lake City, Utah) was used for all statistical analyses.

RESULTS

Two formulations of NPs were created for this study. The first formulation was a biotinylated particle with the following characteristics: average of 14,900 Gd atoms/NP, average diameter of 125.2 nm, and an average relaxivity of 37.1 mmol/$l^{-1}s^{-1}$. The second formulation included fluorescent NBD-labeled or rhodamine-labeled biotinylated particle with the following characteristics: average of 13,800 Gd atoms/NP, average diameter of 125.2 nm, and an average relaxivity of 36.0 mmol/$l^{-1}s^{-1}$.

Activated human monocytes were incubated for 24 h at 37°C with control media, NBD-labeled (green) untargeted particles (1 mmol/l Gd), rhodamine-labeled (red) anti-CD36 particles (1 mmol/l Gd), and a combination of untargeted and targeted particles (2 mmol/l Gd). Cells were then prepared for confocal microscopy, and the remaining cells were counted and sent to ICP-MS for determination of Gd concentrations with normalization for cell number. As seen in Figure 1, there is clear uptake of the red rhodamine-labeled anti-CD36 particles by activated lipid-rich human monocyte-derived macrophages as demonstrated by both confocal microscopy and ICP-MS Gd quantification. As shown, there was only limited uptake of NBD-labeled untargeted particle.

Mean SNR values for pre- and post-contrast T1 images are presented in Table 1 for each aorta section grouped according to whether incubated with untargeted, CD36-labeled, or unspecific-Fc particles. An ANOVA demonstrated no significant difference between mean SNR of aorta groups before incubation with contrast agents (Table 1). Pre- and post-contrast T1 analysis demonstrated that targeted NPs increased CNR by 52.5% (20.3 ± 1.8 vs. 30.9 ± 3.0, $p < 0.0001$), whereas Fc-particles increased CNR by 17.2% (20.7 ± 1.0 vs. 24.2 ± 0.6, $p < 0.0001$), and untargeted particles increased CNR by 18.7% (21.7 ± 1.3 vs. 25.7 ± 1.3, $p < 0.0001$). Matched pre- and post-contrast MR images of aortas treated with untargeted, CD36-labeled, and unspecific-Fc particles can be

Table 1. Pre- and Post-Contrast SNR Values and CNR Values

Variable	Pre-Contrast SNR	Post-Contrast SNR	CNR	Paired *t* Test	2-Way ANOVA
Targeted NPs					
Aorta 1	20.2 ± 2.9	32.9 ± 7.3			
Aorta 2	21.5 ± 0.6	31.8 ± 1.0			
Aorta 3	22.7 ± 0.7	33.3 ± 0.5			
Aorta 4	17.8 ± 0.4	26.1 ± 0.4			
Aorta 15	20.2 ± 0.5	31.2 ± 1.0			
Aorta 16	19.0 ± 0.2	28.8 ± 0.1			
Average	20.3 ± 1.8	30.9 ± 3.0	52.5%	$t = -15.3$, $p < 0.0001$	
Untargeted NPs					
Aorta 5	20.4 ± 2.8	24.8 ± 2.8			
Aorta 6	23.0 ± 0.6	27.5 ± 1.6			
Aorta 7	23.3 ± 0.3	26.9 ± 0.2			
Aorta 8	21.2 ± 0.4	24.4 ± 0.6			
Aorta 13	21.6 ± 0.3	25.7 ± 0.6			
Aorta 14	20.2 ± 0.4	24.1 ± 0.6			
Average	21.7 ± 1.3	25.7 ± 1.3	18.7%	$t = -14.3$, $p < 0.0001$	
Fc-NPs					
Aorta 9	19.9 ± 3.2	23.7 ± 3.2			
Aorta 10	20.6 ± 0.4	24.0 ± 0.4			
Aorta 11	21.5 ± 0.1	25.0 ± 0.2			
Aorta 12	21.2 ± 0.3	24.3 ± 0.5			
Average	20.7 ± 1.0	24.2 ± 0.6	17.2%	$t = -15.3$, $p < 0.0001$	F-ratio = 16.1, $p < 0.0001$
1-way ANOVA	F-ratio = 1.50, p 0.26	F-ratio = 15.6, $p < 0.0004$			

Numbers are expressed as mean ± SD. Pre- and post-contrast signal-to-noise ratio (SNR) values and contrast-to-noise ratio (CNR) values demonstrating the degree of aortic plaque enhancement with gadolinium (Gd)-loaded nanoparticles (NPs) targeting macrophage scavenger receptor-B (CD36), Fc-NPs, and untargeted NPs.
ANOVA = analysis of variance.

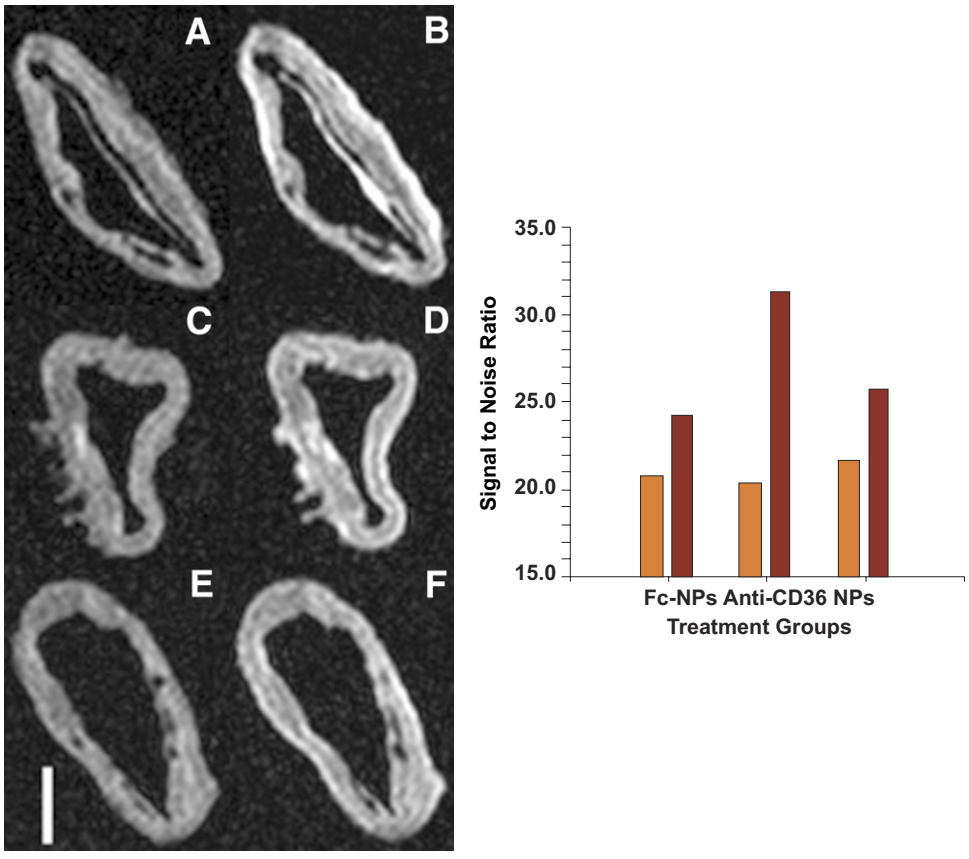

Figure 2. Pre- and Post-Contrast CMR of Aorta Incubated With NPs

Comparison of pre- and post-contrast T1 images of aortas treated with Gd-loaded NPs targeting CD36 (**A and B** respectively), untargeted NPs (**C and D**, respectively), and Fc-NPs (**E and F**, respectively). Included in the bottom left corner is a **scale bar** that represents 1 cm in length. The **error bar graph** included beside **A to F** provides a graphical representation comparing pre- **(orange bars)** and post-contrast signal-to-noise ratio **(brown bars)** seen between aorta sections incubated with targeted NPs, untargeted NPs, and Fc-NPs. CMR = cardiac magnetic resonance; other abbreviations as in Figure 1.

seen in Figure 2 and illustrate the greater increase in signal intensity seen with CD36-labeled particles relative to the untargeted and unspecific particle formulations. The CD36-labeled particles increased CNR significantly when compared with Fc-NPs (F-ratio 33.8, $p < 0.0003$) or when compared with the untargeted analogue (F-ratio 45.0, $p < 0.0001$) on 2-way ANOVA. However, the CNR was not significantly different between aortas treated with untargeted and unspecific-Fc particles (F-ratio 2.25, $p = 0.18$).

Confocal fluorescence microscopy was performed on aortas incubated in NBD-labeled untargeted, CD36-labeled, and unspecific-Fc particles. As shown in Figure 3, red-fluorescent RPE-labeled anti-CD68, an antibody proven to specifically target macrophage lysosomes (15), colocalizes with green-fluorescent NBD-labeled targeted particles in the plaque. Because the macrophages are no longer viable, the colocalization likely represents binding of targeted NPs to CD36 expressed on the surface of resident macrophages in the atherosclerotic plaque. A corresponding light microscopic image reveals that the resident macrophages are heavily present in a small atheroma with a thin fibrous cap. Figure 4 demonstrates confocal microscopy of aortic atherosclerotic plaques treated with untargeted and unspecific-Fc NPs. It demonstrates nonspecific distribution of these formulations within the aortic plaque. Although there is nonspecific distribution in the atherosclerotic plaque with CD36-labeled particles, there is significant binding to macrophages as previously shown. The control aorta demonstrates nuclear staining with DAPI and the staining of macrophages with red-fluorescent RPE-labeled anti-CD68.

Cluster analysis was performed by measuring SNR on pre- and post-contrast T1 images in the

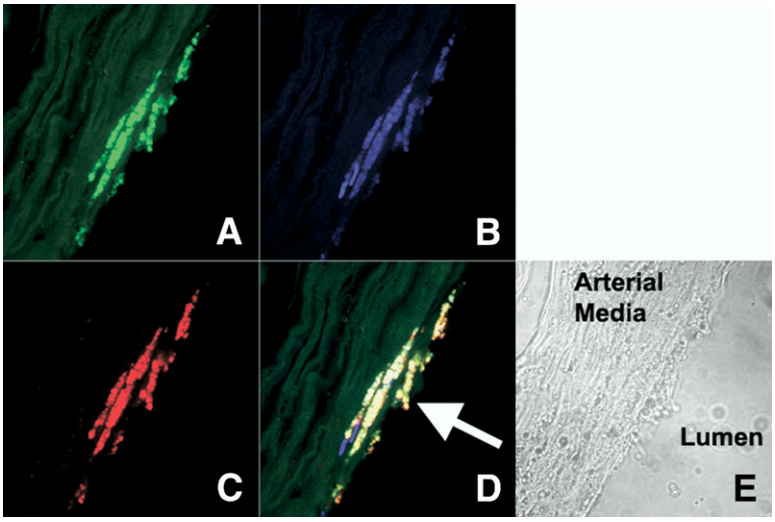

Figure 3. Confocal Microscopy of Atherosclerotic Plaque Demonstrating Fluorescent Macrophage-Specific NPs

Confocal microscopy images of aortic atherosclerotic plaque incubated with **(A)** NBD-labeled **(green)** NPs targeting CD36, **(B)** DAPI (**blue**), **(C)** phycoerythrin (RPE)-labeled **(red)** anti-CD68 (macrophage lysosomes). The merged image **(D)** demonstrates colocalization of NDB-labeled NPs targeting CD36 (macrophage scavenger receptor) and RPE-labeled anti-CD68. The **arrow** points to an atheroma with high macrophage content and thin fibrous cap. **(E)** Corresponding light microscope image. Abbreviations as in Figure 1.

lipid core or fibrous cap on the basis of comparison of composition images with histopathological images stained with hematoxylin and eosin. Image comparison can be seen in Figure 5. Pre- and post-contrast SNR data for fibrous cap and lipid core are available in Table 2. A 2-way ANOVA demonstrated that there was a greater increase in SNR in the fibrous cap compared with the lipid core after incubation with CD36-labeled NPs (75.2% vs. 43.7%, respectively, $p < 0.0003$). However, there was a greater increase of SNR in the lipid core compared with the fibrous cap after incubation with untargeted (24.7% vs. 16.9%, respectively, $p < 0.0001$) and unspecific-Fc particles (22.5% vs. 15.1%, respectively, $p < 0.01$). Aortic plaque incubated with the CD36-labeled particles seemed to have the greatest increase in signal intensity in regions with a large number of resident macrophages bound by NBD-labeled targeted NPs (Fig. 3).

DISCUSSION

The findings of this study demonstrate that Gd-loaded NPs targeting CD36, a class B scavenger receptor, were able to specifically target human macrophages in vitro as demonstrated by confocal microscopy and ICP-MS. Anti-CD36 NPs had significantly greater CNR in cadaveric human aortic atherosclerosis than untargeted and unspecific-Fc particles on T1 MR images. Additionally, fluorescent confocal microscopy validated that NBD-labeled, CD36-labeled particles targeted resident macrophages through colocalization of NBD-labeled targeted NPs and RPE-labeled anti-CD68. Whereas untargeted and unspecific-Fc particles were shown to be nonspecifically distributed throughout the atherosclerotic plaque on confocal microscopy, the CD36-labeled particles both specifically targeted the macrophages and were also nonspecifically distributed throughout the plaque. Finally, this study demonstrates that that the CD36-labeled particles had a greater CNR on T1 images in fibrous plaque, whereas untargeted and unspecific-Fc particles had a greater CNR on T1 images in lipid-rich plaque. The greatest increase in the fibrous plaque with CD36-targeted particles seemed to occur on periphery of the lipid-rich plaque through binding to macrophages surrounding the lipid-rich core.

Targeted imaging of macrophages as a possible means of detecting and characterizing atherosclerosis has been investigated with multiple imaging modalities (18). The use of CD36-labeled particles that specifically target the macrophage scavenger receptor to detect atherosclerosis with CMR was previously investigated in a murine model of atherosclerosis (8,9). The targeted NPs were shown to specifically target CD204 (macrophage scavenger

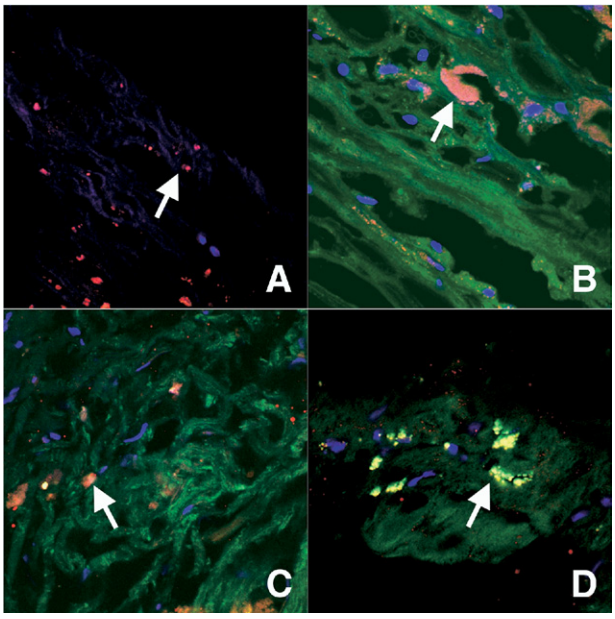

Figure 4. Confocal Microscopy of Plaque Demonstrating Uptake of NPs

Confocal microscopy merged images (NBD = **green**, anti-CD68 = **red**, DAPI = **blue**) at 100× of atherosclerotic plaque incubated with **(A)** control (non-fluorescent untargeted NPs), **(B)** NBD-labeled untargeted NPs, **(C)** NBD-labeled Fc-NPs, **(D)** and NBD-labeled targeted NPs. The images were of the intimal plaque and therefore do not have the auto-fluorescence of the internal elastic lamina and media. There was no green fluorescence seen in control aortic plaque incubated with non-fluorescent untargeted NPs, whereas nonspecific distribution of NBD-labeled untargeted NPs, Fc-NPs, and targeted NPs can be seen throughout the plaque. An **arrow** is present in each image to identify resident macrophages. Significant colocalization was seen of NBD-labeled targeted NPs and anti-CD68 **(D)**, whereas significant colocalization was not seen with NBD-labeled untargeted NPs and Fc-NPs **(B and C)**. This suggests that macrophages are bound by targeted NPs targeting CD36.

receptor types I and II) and resulted in increased binding and uptake in murine macrophages (8). Incubation of cells with oxidized low-density lipoprotein and excess anti-CD204 were both shown to reduce binding of targeted NPs targeting CD-204 (8). Additionally, ex vivo imaging of murine aortic atherosclerosis after incubation with contrast agents (8) and in vivo aortic plaque MR imaging in mice injected with contrast agent (9) revealed that greater enhancement of the atherosclerotic plaque occurs with targeted NPs compared with non-targeted NPs and targeted NPs specifically bound resident macrophages in the plaque. In the current study, we employed rabbit anti-human antibodies targeting CD36, a member of the class B scavenger receptor family. Both CD36 and MSR-A have been shown to play a role in the development of atherosclerosis and collectively are responsible for binding and uptake of 75% to 90% of modified low-density lipoprotein uptake by macrophages (19). Several studies have highlighted the importance of CD36 for plaque development by demonstrating significant reduction in the short-term and long-term development of atherosclerosis in mice with apolipoprotein (Apo)-E knockout and CD36 knockout compared with Apo-E knockout mice (20,21). Additionally, transplantation of stem cells with CD36 in the double knockout mice ($CD36^{-/-}$, $Apo\text{-}E^{-/-}$) resulted in increased development of atherosclerosis (22). However, Moore et al. (23) found that Apo-E knockout mice lacking CD36 had greater aortic sinus atherosclerosis development than Apo-E knockout mice. This study demonstrates the potential to use molecular MR imaging with NPs targeting CD36 to improve the detection and characterization of atherosclerotic plaque and might serve as a way to investigate the role of CD36 in the progression or regression of atherosclerosis.

Detection of atherosclerosis with CMR has also been achieved with superparamagnetic iron oxide particles (SPIOs). Although studies have demonstrated that SPIOs are taken up by macrophages in atherosclerotic plaque, a recent study investigated the mechanism of cellular uptake of SPIOs. von Zur Muhlen et al. (24) demonstrated that the integrin Mac-1 is crucial in the uptake of SPIOs, and binding/uptake was significantly reduced after blocking Mac-1 with antibodies targeting CD11b. Ultra-small SPIOs have been shown to detect inflamed carotid atherosclerotic plaques with correlation to macrophage density (25). Additionally, echogenic imaging agents could be developed to target macrophages in atherosclerotic plaque and enhance plaque detection and characterization. Nuclear imaging with positron emission tomography and single-photon emission computed tomography with imaging agents taken up by macrophages and foam cells might enable detection and characterization of inflamed atherosclerotic plaque (26). Finally, targeted imaging of macrophages with contrast agents for computed tomography (27), optical imaging, or with multimodal imaging agents (28) seems very promising.

One limitation of this study is that the imaging was not performed on viable aorta due to the ex vivo study design in which the aorta was harvested at the time of autopsy from human subjects. However, our data demonstrate uptake of targeted and untargeted NPs by human macrophages in vitro. Additionally, we did not determine the role particle diffusion played in our study and whether there was greater binding at the

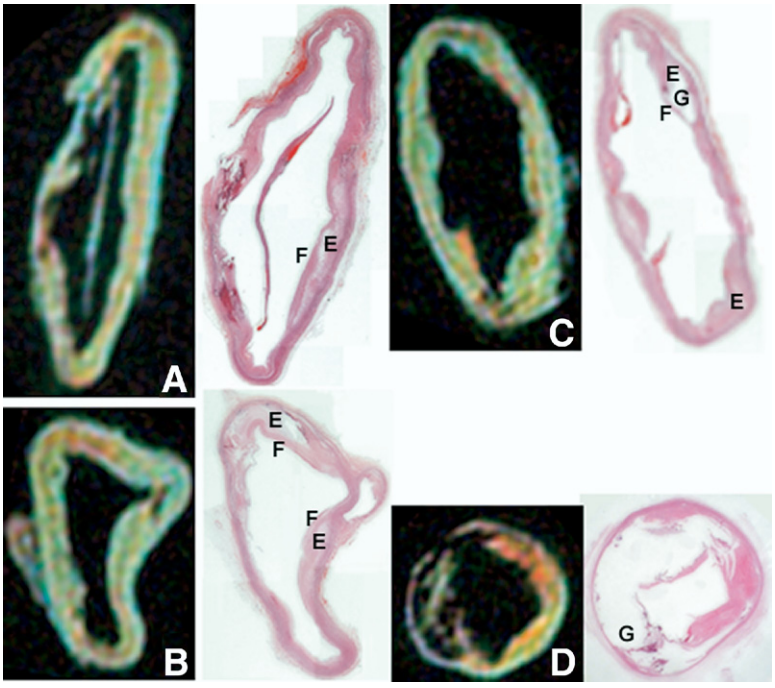

Figure 5. CMR Composition Images Compared With Histopathology of Aortic Plaque

The top image is a composition image created by merging T1 image converted to **red**, T2 converted to **green**, and proton-density-weighted converted to **blue**. The figure provides a comparison of the composition images with the corresponding light microscope images stained with hematoxylin. Aorta specimens were incubated for 24 h with targeted NPs **(A)**, untargeted NPs **(B and D)**, and Fc-NPs **(C)**. With histopathological comparison, it is possible to determine regions of the plaque such as the lipid-rich core **(E)**, the fibrous cap **(F)**, and heavily calcified regions of the plaque **(G)**. The aorta represented in **D** is an example of a heavily calcified aorta consistent with a type Vb classification, whereas aorta specimens in images **A, B, and C** tend to have numerous type IV and Va lesions. Abbreviations as in Figure 1.

surface compared with more central or deep macrophages. Staining for MSR-A would have provided additional information regarding the expression of other scavenger receptors on the surface of macrophages in the aortic atherosclerotic plaque and enable comparison with prior studies that investigated scavenger receptor expression (29). Another limitation in the use of particles targeting CD36 is that intravenous administration of this imaging agent will suffer first pass effect in the liver by binding to scavenger receptors expressed on the surface of Kuppfer cells (18). Toxicity data for the lipid-based particle platform are also lacking; however, studies indicate that liver uptake of the Gd-labeled particles might limit clinical translation (30). Similarly, this study only evaluated colocalization with macrophages and did not assess bind-

Table 2. Pre- and Post-Contrast SNR Values of the Fibrous Cap and the Lipid Core in Human Aortic Atherosclerosis

Variable	Pre-Con SNR	Post-Con SNR	CNR	*t* value	p Value
Fibrous cap					
Targeted NPs	23.8 ± 0.5	41.7 ± 1.2	75.2%	−24.3	<0.0001
Untargeted NPs	23.6 ± 0.5	27.6 ± 0.7	16.9%	−28.8	<0.0001
Fc-NPs	23.9 ± 0.5	27.5 ± 0.5	15.1%	−8.9	<0.001
Lipid core					
Targeted NPs	16.7 ± 0.8	24.0 ± 1.1	43.7%	−19.8	<0.0001
Untargeted NPs	17.0 ± 0.5	21.2 ± 0.5	24.7%	−48.1	<0.0001
Fc-NPs	16.5 ± 0.2	20.2 ± 0.6	22.5%	−20.4	<0.0001

Pre- and post-contrast SNR values of the fibrous cap and the lipid core in human aortic atherosclerosis incubated with targeted NPs, untargeted NPs, and Fc-NPs. This table enables determination, for each contrast agent, of whether CNR is greater in the fibrous cap or the lipid core. Numbers are expressed as mean ± SD.
Abbreviations as in Table 1.

JACC: CARDIOVASCULAR IMAGING, VOL. 2, NO. 5, 2009
MAY 2009:637–47

ing of anti-CD36 targeted particles to other cells that express CD36, such as endothelial cells, smooth muscle cells, adipocytes, and platelets. An additional limitation of this agent in its current form is the use of rabbit antibodies targeting human CD36. These antibodies will likely result in an immune response against the antibody portion of the imaging agent and would therefore limit the use of this agent in tracking progression/regression of atherosclerotic plaque. Future studies should include isotype-matched antibodies to further test specificity of the antibody targeting. Finally, the role of imaging with NPs targeting CD36 remains to be validated for in vivo atherosclerotic plaque detection.

CONCLUSIONS

Gd-loaded lipid-based NPs targeting CD36, a class B scavenger receptor, had significant uptake by human macrophages in vitro, improved signal intensity of ex vivo aortic atherosclerotic plaque, and were shown to bind to resident macrophages in atherosclerotic plaque on confocal microscopy. Finally, the CD36-labeled particles created the largest signal intensity in regions of fibrous plaque on the periphery of lipid-rich plaque. These data suggest that lipid-based NPs targeting CD36 might improve detection and characterization of atherosclerotic plaque and determine the degree of plaque inflammation by assessing macrophage density.

Reprint requests and correspondence: Dr. Zahi A. Fayad, Mount Sinai School of Medicine, One Gustave L. Levy Place, Imaging Science Laboratories, Box 1234, New York, New York 10029. *E-mail: zahi.fayad@mssm.edu.*

REFERENCES

1. American Heart Association. Heart Disease and Stroke Statistics—2006 Update. Dallas, TX: The American Heart Association, 2006.
2. Ambrose JA, Tannenbaum MA, Alexopoulos D, et al. Angiographic progression of coronary artery disease and the development of myocardial infarction. J Am Coll Cardiol 1988;12:56–62.
3. Little WC, Constantinescu M, Applegate RJ, et al. Can coronary angiography predict the site of a subsequent myocardial infarction in patients with mild-to-moderate coronary artery disease? Circulation 1988;78:1157–66.
4. Topol EJ, Nissen SE. Our preoccupation with coronary luminology. The dissociation between clinical and angiographic findings in ischemic heart disease. Circulation 1995;92:2333–42.
5. Davies MJ, Richardson PD, Woolf N, Katz DR, Mann J. Risk of thrombosis in human atherosclerotic plaques: role of extracellular lipid, macrophage, and smooth muscle cell content. Br Heart J 1993;69:377–81.
6. Carr S, Farb A, Pearce WH, Virmani R, Yao JS. Atherosclerotic plaque rupture in symptomatic carotid artery stenosis. J Vasc Surg 1996;23:755–65, discussion 765–6.
7. Lipinski MJ, Fuster V, Fisher EA, Fayad ZA. Technology Insight: targeting of biological molecules for evaluation of high-risk atherosclerotic plaques with magnetic resonance imaging. Nat Clin Pract Cardiovasc Med 2004;1:48–55.
8. Lipinski MJ, Amirbekian V, Frias JC, et al. MRI to detect atherosclerosis with gadolinium-containing immunomicelles targeting the macrophage scavenger receptor. Magn Reson Med 2006;56:601–10.
9. Amirbekian V, Lipinski MJ, Briley-Saebo KC, et al. Detecting and assessing macrophages in vivo to evaluate atherosclerosis noninvasively using molecular MRI. Proc Natl Acad Sci U S A 2007;104:961–6.
10. Kimpe K, Parac-Vogt TN, Laurent S, et al. Potential MRI contrast agents based on micellar incorporation of amphiphilic bis(alkylamide) derivatives of [(Gd-DTPA)(H2O)]2-. Eur J Inorg Chem 2003;2003:3021–7.
11. Winter PM, Caruthers SD, Yu X, et al. Improved molecular imaging contrast agent for detection of human thrombus. Magn Reson Med 2003;50:411–6.
12. Bannon PG, Dean RT, Dawes J. Isolation and maintenance of nonadherent quiescent human monocytes for studies of adhesion and migration. Methods in Cell Science 1995;17:53–9.
13. Briley-Saebo KC, Shaw PX, Mulder WJ, et al. Targeted molecular probes for imaging atherosclerotic lesions with magnetic resonance using antibodies that recognize oxidation-specific epitopes. Circulation 2008;117:3206–15.
14. Itskovich VV, Samber DD, Mani V, et al. Quantification of human atherosclerotic plaques using spatially enhanced cluster analysis of multicontrast-weighted magnetic resonance images. Magn Reson Med 2004;52:515–23.
15. Holness CL, Simmons DL. Molecular cloning of CD68, a human macrophage marker related to lysosomal glycoproteins. Blood 1993;81:1607–13.
16. Hajduk SL. Demonstration of kinetoplast DNA in dyskinetoplastic strains of Trypanosoma equiperdum. Science 1976;191:858–9.
17. Stary HC, Chandler AB, Dinsmore RE, et al. A definition of advanced types of atherosclerotic lesions and a histological classification of atherosclerosis. A report from the Committee on Vascular Lesions of the Council on Arteriosclerosis, American Heart Association. Arterioscler Thromb Vasc Biol 1995;15:1512–31.
18. Lipinski MJ, Frias JC, Fayad ZA. Advances in detection and characterization of atherosclerosis using contrast agents targeting the macrophage. J Nucl Cardiol 2006;13:699–709.
19. Kunjathoor VV, Febbraio M, Podrez EA, et al. Scavenger receptors class A-I/II and CD36 are the principal receptors responsible for the uptake of modified low density lipoprotein leading to lipid loading in macrophages. J Biol Chem 2002;277:49982–8.
20. Guy E, Kuchibhotla S, Silverstein R, Febbraio M. Continued inhibition of atherosclerotic lesion development in long term Western diet fed CD36o/apoEo mice. Atherosclerosis 2007;192:123–30.
21. Febbraio M, Podrez EA, Smith JD, et al. Targeted disruption of the class B scavenger receptor CD36 protects against atherosclerotic lesion development in mice. J Clin Invest 2000;105:1049–56.

22. Febbraio M, Guy E, Silverstein RL. Stem cell transplantation reveals that absence of macrophage CD36 is protective against atherosclerosis. Arterioscler Thromb Vasc Biol 2004;24:2333–8.
23. Moore KJ, Kunjathoor VV, Koehn SL, et al. Loss of receptor-mediated lipid uptake via scavenger receptor A or CD36 pathways does not ameliorate atherosclerosis in hyperlipidemic mice. J Clin Invest 2005;115:2192–201.
24. von Zur Muhlen C, von Elverfeldt D, Bassler N, et al. Superparamagnetic iron oxide binding and uptake as imaged by magnetic resonance is mediated by the integrin receptor Mac-1 (CD11b/CD18): Implications on imaging of atherosclerotic plaques. Atherosclerosis 2006;193:102–11.
25. Trivedi RA, Mallawarachi C, U-King-Im JM, et al. Identifying inflamed carotid plaques using in vivo USPIO-enhanced MR imaging to label plaque macrophages. Arterioscler Thromb Vasc Biol 2006;26:1601–6.
26. Davies JR, Rudd JH, Weissberg PL, Narula J. Radionuclide imaging for the detection of inflammation in vulnerable plaques. J Am Coll Cardiol 2006;47:C57–68.
27. Hyafil F, Cornily JC, Feig JE, et al. Noninvasive detection of macrophages using a nanoparticulate contrast agent for computed tomography. Nat Med 2007;13:636–41.
28. Sosnovik DE, Nahrendorf M, Deliolanis N, et al. Fluorescence tomography and magnetic resonance imaging of myocardial macrophage infiltration in infarcted myocardium in vivo. Circulation 2007;115:1384–91.
29. Nakata A, Nakagawa Y, Nishida M, et al. CD36, a novel receptor for oxidized low-density lipoproteins, is highly expressed on lipid-laden macrophages in human atherosclerotic aorta. Arterioscler Thromb Vasc Biol 1999;19:1333–9.
30. Briley-Saebo KC, Amirbekian V, Mani V, et al. Gadolinium mixed-micelles: effect of the amphiphile on in vitro and in vivo efficacy in apolipoprotein E knockout mouse models of atherosclerosis. Magn Reson Med 2006;56:1336–46.

Key Words: atherosclerosis ■ CD36 ■ macrophage ■ magnetic resonance imaging ■ nanoparticles.